ACS APPLIED MATERIALS & INTERFACES

RESEARCH ARTICLE

www.acsami.org

Fabricating Superhydrophobic Polymer Surfaces with Excellent Abrasion Resistance by a Simple Lamination Templating Method

Qian Feng Xu, Bikash Mondal, and Alan M. Lyons*

Department of Chemistry, College of Staten Island, City University of New York, Staten Island, New York 10314, United States

Supporting Information

ABSTRACT: Fabricating robust superhydrophobic surfaces for commercial applications is challenging as the fine-scale surface features, necessary to achieve superhydrophobicity, are susceptible to mechanical damage. Herein, we report a simple and inexpensive lamination templating method to create superhydrophobic polymer surfaces with excellent abrasion resistance and water pressure stability. To fabricate the surfaces, polyethylene films were laminated against woven wire mesh templates. After cooling, the mesh was peeled from the polymer creating a 3D array of ordered polymer microposts on the polymer surface. The resulting texture is monolithic with the polymer film and requires no chemical modification to exhibit superhydrophobicity. By controlling lamination parameters and mesh dimensions, polyethylene surfaces were fabricated that exhibit static contact angles of 160° and slip angles of 5°. Chemical and mechanical stability was evaluated using an array of manual tests as well as a standard reciprocating abraser test. Surfaces remained superhydrophobic after more than 5500 abrasion cycles at a pressure of 32.0 kPa. In addition, the surface remains dry after immersing into water for 5 h at 55 kPa. This method is environmental friendly, as it employs no solvents or harsh chemicals and may provide an economically viable path to manufacture large areas of mechanically robust superhydrophobic surfaces from inexpensive polymers and reusable templates.

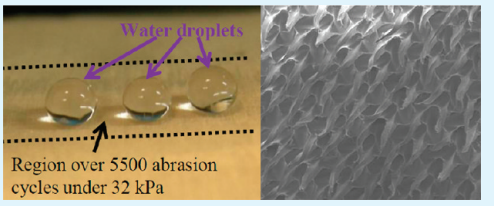

KEYWORDS: superhydrophobic surface, polymer, abrasion resistance, underwater stability, lamination templating

1. INTRODUCTION

Many plants and animals naturally form superhydrophobic surfaces. Well-known examples include the lotus (*Nelumbo nucifera*) with self-cleaning leaves and water striders (*Gerris remigis*) that are able to walk on the surface of water.[1,2] Models to explain superhydrophobic phenomena were first published by Wenzel and Cassie−Baxter and have subsequently been refined.[3−7] In general, to achieve surfaces that exhibit contact angles with water exceeding 150° and slip angles below 10°, a hydrophobic surface needs to be created with significant surface roughness. In this way, water is suspended between adjacent surface features such that the droplet surface is primarily surrounded by air and is in contact with a relatively small areal fraction of the solid substrate.[8−10] Surfaces with this structure exhibit many interesting properties, not commonly observed on most natural or synthetic surfaces, including the ability for water droplets to easily slip along the surface. These properties have motivated the search for superhydrophobic materials that satisfy the requirements of a range of commercial applications including surfaces that exhibit reduced drag and corrosion protection, as well as materials for advanced textiles.[11−25] However, for synthetic superhydrophobic surfaces to have commercial viability, they must exhibit mechanical and chemical stability as well as significant abrasion resistance.[11,12]

A wide variety of approaches to fabricating superhydrophobic surfaces has been reported and reviewed.[11−15] Some artificial surfaces with superoleophobic properties have also been successfully fabricated.[26−30] Although techniques for forming these surfaces are numerous, most of these processes are expensive, require many steps, and are limited to producing small areas. Moreover, because a surface with high roughness tends to be delicate and thus easily damaged, superhydrophobic properties are rapidly lost when touched. For example, if a synthetic superhydrophobic surface or the surface of lotus leaf is touched with a bare hand, the affected area of the surface could be contaminated by salt and oil and the surface energy of the touched area would increase dramatically. The force exerted by touching would also damage the fragile topology of the surface and the touched area would permanently lose its superhydrophobicity. As a result, the relatively poor abrasion resistance of superhydrophobic surfaces severely limits their commercial implementation.

Several approaches to improving the robustness of superhydrophobic surfaces have recently been reported. For example, a superhydrophobic surface that is stable to repeated laundering cycles was made using simultaneous γ radiation to graft a fluorinated acrylate monomer onto the surface of a cotton fabric.[31] Although the laundering performance reportedly improved, the abrasion resistance behavior was not reported. A few groups have reported superhydrophobic surfaces[32−35] that are relatively stable, however they are still far from meeting the requirements for practical industrial applications. Abrasion resistance of a polyurethane elastomer fabricated by molding against a sacrificial

Received: June 8, 2011
Accepted: July 28, 2011
Published: July 28, 2011

dx.doi.org/10.1021/am200741f | ACS Appl. Mater. Interfaces 2011, 3, 3508–3514

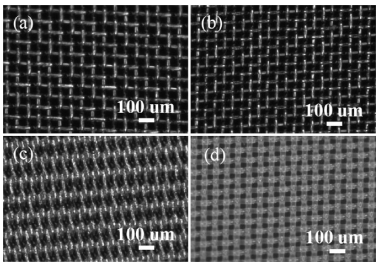

Figure 1. Optical images of mesh templates used for fabricating robust superhydrophobic surfaces, (a) M1, (b) M2, (c) M3, (d) M4.

aluminum oxide template[36] was found to maintain a contact angle above 150° after 10,000 cycles, however the surface was exposed to a very modest pressure of less than 3 kPa (<0.5 psi). Furthermore, the sacrificial templates would be expensive to fabricate. A nanotextured silicon surface[37] has been reported to be resistant to abrasion, but again, the magnitude of the abrasion is low (<3.5 kPa) and limited to one cycle. In this study, several different superhydrophobic surfaces were tested concurrently, including polyurethane and PTFE, and their properties were found to degrade significantly by this test.[37] Thus there is a need to develop new materials that are inexpensive to fabricate and that maintain their superhydrophobic properties after the high abrasion levels commonly encountered in commercial applications.

Herein we describe a simple and inexpensive lamination templating method which is used to create superhydrophobic polymer surfaces with excellent abrasion resistance. A mesh cloth, woven from either steel or polymeric filaments, is employed as a reusable template. The polymer film is laminated against this template under elevated heat and pressure. After removal from the press, the template mesh is peeled cleanly from the polymer film leaving a highly textured surface. The fabricated polymer surfaces are composed of 3D ordered micropost arrays and show superhydrophobicity immediately without any further surface modification (static water CA of 160° and a slip angle of less than 5°). Different from many other microfabrication methods, the 3D polymer microposts are monolithic with the substrate and so are not adhesively attached. Because they are formed by mechanical stretching a crystalline polymer, they exhibit significant toughness. As a result, the templated surface is very robust and abrasion resistant. The materials maintain water repellency after repeated abrasion cycles, as well as washing, scrubbing and ultrasonicating with a saturated solution of industrial cleansers. The effect of mesh template (wire diameter, pore diameter, and weave) and lamination conditions (temperature and pressure) on surface morphology and wetting properties will be discussed.

2. EXPERIMENTAL SECTION

Materials, Methods, and Surface Fabrication. A commercially available thermoplastic sheet of low density polyethylene (LDPE) manufactured by Berry Plastics from 97% recycled polyethylene, 2% calcium carbonate and 1% slip oleamide and sold through McMaster-Carr was used as the polymer substrate. The thickness of the LDPE film was 100 μm and 10 layers were used at each time to make free-standing superhydrophobic sheets that are approximately 1 mm thick. The polymer film softens at 106 °C and melts over the range from 113 to 120 °C (see DSC curve in Supporting Information figure SF1). Three types of stainless steel mesh and one type of Nylon mesh (all from McMaster-Carr) with different wire diameters and pore sizes were used as templates. The structures and details of the mesh are shown in Figure 1 and Table 1. The procedure for fabricating surfaces involves two processing steps as shown schematically in Figure 2. In the first step, a stack of LDPE sheets and a mesh template are laminated together under heat and pressure with the targeted polymer surface facing the mesh template. The stack-up was heated above its softening temperature (~105 °C) under pressure for 3−30 min. In the second step, the template is separated from the polymer film. The laminated stack was cooled to 25 °C and then the mesh was separated from the polymer surface by peeling. The fabricated superhydrophobic surface is formed and exposed during the peeling process. As the LDPE did not adhere to the stainless steel or Nylon mesh, the template could be reused.

Table 1. Parameters of Mesh Templates for Fabricating Superhydrophobic Surfaces

mesh no.	wire diameter 1 (μm)	wire diameter 2 (μm)	square pore side length (μm)	open area (%)
M1, 325 mesh	28	28	50	41
M2, 400 mesh	25	25	38	36
M3, 200 × 1400 mesh	71	41	10	2
M4, 371 mesh	33	33	36	28

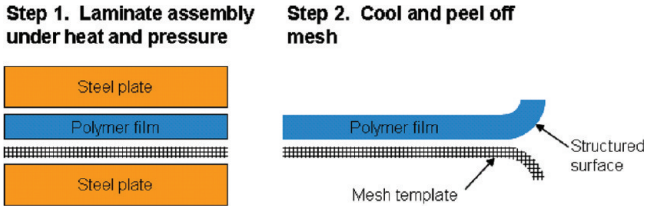

Figure 2. Schematic of the lamination peeling process.

Characterization. The surface structures were studied by field emission scanning electron microscopy (FESEM, Amary) and optical microscopy (Nikon-SMZ 1500 and Laborlux-12ME). The static contact angles (CAs) and slip-off angle were measured with a goniometer (250-F1, Rame-Hart Instruments Co). Droplets of distilled water, with a volume of 2−5 μL, were placed gently onto the surface at room temperature and pressure. The static CA and advancing and receding CAs were measured five times at different locations such that the measurement variance was ±2°. The slip-off angle was determined by measuring the substrate angle at which water droplets (~10 μL) placed on the surface with a micro syringe needle would roll off the surface.

Abrasion Tests. Abrasion resistance of the fabricated surface was evaluated using both a multistep manual test as well as a standard reciprocating abrasion testing machine. The manual multistep test includes a sequence of four steps: (1) dry abrading firmly with a gloved hand (Showa Best Glove part 6005PF) using a back and forth movement for 50 times, (2) dry abrading firmly with a hand wearing an industrial cotton glove back and forth for 50 times, (3) wet scrubbing manually with a gloved finger for 1 h (20 cycles @ 2−4 min/cycle) with a saturated industrial cleaner solution (ALCONOX - Powdered Precision Cleaner, containing 7−13% sodium carbonate, 10−30% sodium dodecylbenzenesulfonate, 10−30% tetrasodium pyrophosphate, and 10−30% sodium phosphate), and (4), ultrasonicating in the same saturated industrial cleaner solution for 5 h (Branson 1200 ultrasonic cleaner, ~150 W).

The mechanized abrasion test was conducted with a Taber model 5900 reciprocating abraser using a CS-8 wearaser abradant, as shown in SF2. The following conditions were used for the abrasion test: the stroke

Table 2. Fabrication Conditions for Surfaces S1−S6 and Their Superhydrophobic Properties

		lamination conditions				superhydrophobicity (deg)			
surface no.	mesh no.	temp (°C)	pressure (kPa)	time (min)	peel temp (°C)	θ_{Static}	θ_{Adv}	θ_{Rec}	θ_{Slip}
S1	M1	115	1400	30	25	125			
S2	M1	120	1400	30	25	160			3
S3	M1	125	1400	3	25	160			5
S4	M2	125	69	15	25	160	163	155	5
S5	M3	125	69	15	25	158			3
S6	M4	125	69	15	25	160	162	157	5

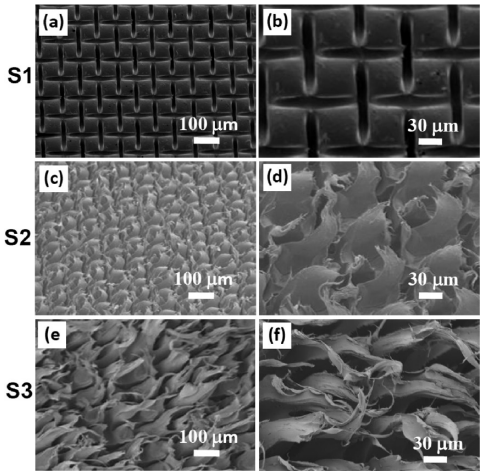

Figure 3. SEM images of surfaces fabricated with mesh 1 (M1) at different temperatures under the same pressure: (a, b) surface S1, 115 °C. (c, d) surface S2, 120 °C, (e, f) surface S3, 125 °C. Panels b, d, and f are higher-magnification views of panels a, c, and e, respectively.

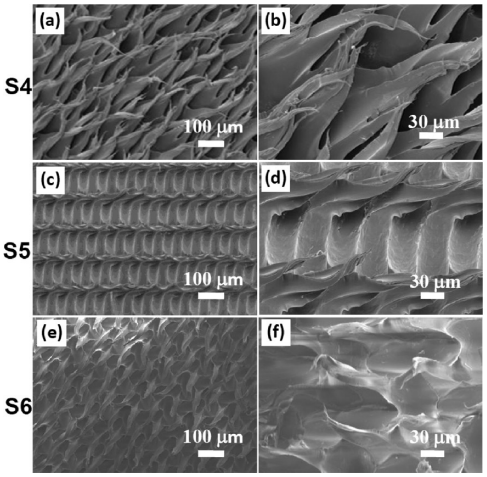

Figure 4. SEM images of surfaces fabricated with different mesh templates at the same lamination temperature and pressure: (a, b) surface S4 made from mesh 2, (c, d) surface S5 made from mesh 3, (e, f) surface S6 made from mesh 4. Panels b, d, and f are the higher-magnification views of panels a, c, and e, respectively.

length was 4 cm, the abrasion linear speed was 8 cm s^{-1}, and the applied pressure was 32.0 kPa (4.64 psi).

Water Pressure Stability Test. A piece of the fabricated superhydrophobic polymer sheet with a size of 25 mm ×38 mm was placed inside a Nordson-EFD polypropylene syringe barrel, immersed in water, and capped with a piston as shown schematically in SF3. The syringe was then pressurized, using a Nordson-EFD regulated dispenser. The reflectivity at the interface between water and the superhydrophobic surface was monitored visually and recorded using a digital camera. After the pressure was relieved, the sample was removed from the water filled syringe and the wetting properties of the surface were measured using optical microscopy (Nikon-SMZ 1500 and Laborlux-12ME).

3. RESULTS AND DISCUSSION

3.1. Surface Fabrication. The procedure for processing polymer films into robust superhydrophobic surfaces is comprised of two main steps, as shown schematically in Figure 2. In the first step, the polymer film and mesh template are laminated together under heat and pressure. For these experiments, a low density recycled polyethylene (LDPE) film was used with a softening point of ∼106 °C. Lamination was conducted at or above the crystalline melting temperature and at a pressure high enough to force the viscous polymer against the wires. At sufficiently high temperatures and pressures, the polymer flowed adequately to infiltrate the wires, forming a thin layer of polymer on the back side of the mesh. Four kinds of mesh, shown in Figure 1, were used as templates to fabricate surfaces; mesh details are listed in Table 1. In the second step, the laminated LDPE-mesh is cooled to room temperature (25 °C) and the mesh is then separated from the polymer by peeling. As the mesh is peeled away, the polymer that had infiltrated the mesh is stretched and elongated until it breaks. Thus the target surface is composed of both an imprint of the wires on the mesh surface as well as an array of high-aspect-ratio features resulting from the polymer that had surrounded the wires and/or filled the pores of the mesh. Detailed fabrication conditions for surfaces S1−S6 are shown in Table 2.

SEM images of superhydrophobic surfaces made using the four different types of mesh under different conditions are shown in Figures 3 and 4. The surfaces are similar in that they are composed of 3D ordered arrays of polymer microposts. The pitch and diameter of the posts correspond to the pitch and opening size of the mesh. When low temperatures are used, however, polymer flow is limited and the template is simply embossed into the polymer surface creating a negative image of the wire mesh as shown for surface S1 in Figure 3a,b. At this low temperature, the LDPE does not flow into the mesh; the wires are forced into the polymer surface. The height of the posts on surface S1 varies with the woven wire as shown in Figure SF4, and is estimated to range from 25 to 45 μm.

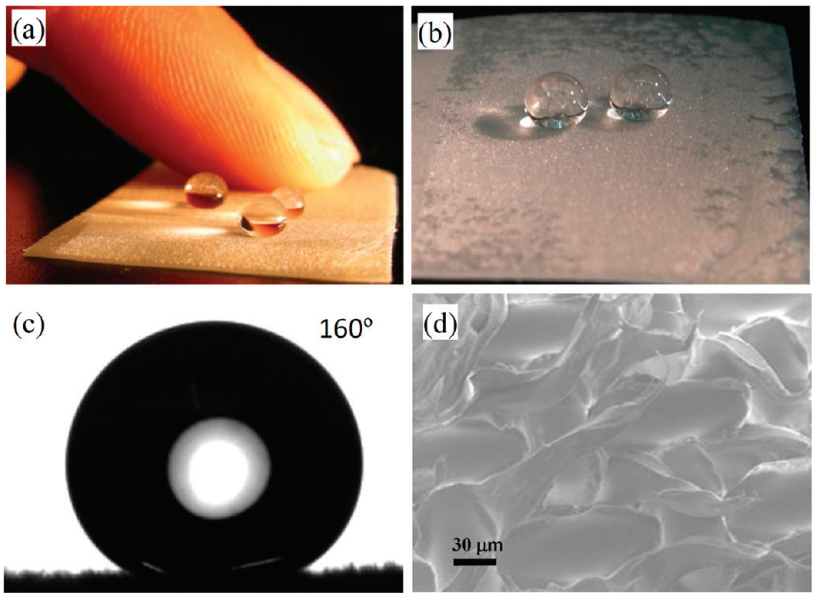

Figure 5. Surface S6 after manual abrasion testing (a) being touched with a bare finger, (b) water droplets on a partly dried surface after the multistep manual test, (c) water contact angle of the surface after the same multistep manual test; the surface was rinsed with water and dried before measuring, (d) SEM image of the surface structure after the same multistep manual test. The surface was rinsed, dried, and coated with gold before imaging.

At higher lamination temperatures, the LDPE flows to a greater extent and penetrates into the mesh to a degree dependent upon the temperature. After peeling, the LDPE surfaces are covered with an array of finely textured features, as shown for surfaces S2—S6 in Figure 3c—f and Figure 4. These surfaces are substantially different from surface S1 as well as from previously reported surfaces that were made by more conventional templating process which more faithfully replicate the geometry of templates.[36,38] This is because the polymer film infiltrates the template during lamination and is stretched until it breaks during peeling. When the temperature was increased to 120 °C, the flowability of the LDPE becomes greater and a thin polymer layer was formed on the backside of the wires. During peeling, the polymer that encapsulated the wires was stretched and broken. This resulted in the formation of surface S2 composed of features with a thin petal-like structure as shown in Figure 3c,d. Surface S3 (Figure 3e,f) was laminated at a still higher temperature (125 °C) under the same pressure. The viscosity of the LDPE at 125 °C is much lower as it is well above the crystalline melt temperature of the polymer. Under the applied pressure, a relatively thick layer of polymer was formed on the backside of the mesh. The flow was sufficiently high that only a 3 min lamination cycle was needed. After peeling, the polymer that had filled the pores was stretched and broken. This created a surface with an array of high aspect ratio spike-like features with a pitch and base dimension comparable to the pitch and size of the pores as shown in Figure 3e,f. Thus the lamination temperature can affect the extent of polymer flow into the mesh which, in turn, significantly affects the structure of the surface features.

Because the viscosity of LDPE is significantly reduced at 125 °C, the lamination also can be done at lower pressures for a longer time, which could be favorable depending upon the lamination equipment available. Surfaces S4—S6 were fabricated with different meshes at 125 °C and a lower pressure for 15 min. The structures of the fabricated surfaces are shown in Figure 4. A 15 min lamination time was used to ensure reproducibility and thermal equilibrium; shorter lamination times could also be used. Surface S4 is similar in structure to surface S3 as both were formed using a stainless steel plain weave mesh, however S4 was made with a finer mesh and so the pitch of the posts is reduced (63 vs 78 μm) and the base size of the spikelike features is smaller (38 vs 50 μm). A nylon mesh was used as the template for surface S6. This created a LDPE surface with relatively smaller features (36 μm pore opening) on a 33 μm pitch. These features are smaller than those created with the plain weave steel mesh (S3 and S4) and occupy a lower percentage of the surface area. Surface S5 is made using a stainless steel mesh woven in a Dutch Twill weave with the smallest pores examined (10 μm) within this group. This weave style creates a very small pore fraction and thus a low density of spiked features which are arrayed into rows.

For all samples, the length of the polymer posts is related to the plasticity of the polymer, the thickness of the mesh and the thickness of the polymer film formed on the backside of mesh. Thus the structure of the fabricated posts can be controlled by adjusting the lamination conditions (e.g., pressure, temperature, and time) as well as the geometry of the mesh templates (e.g., the wire diameter and the pore size). Infiltration of an open, porous template creates surfaces with few defects because air can pass through the mesh and is not trapped in blind openings as can occur with closed pore templates. The directional orientation of the polymer posts is related to the angle between the mesh and the polymer sheet during peeling.

3.2. Superhydrophobicity. The wetting behavior of the fabricated surfaces was studied by measuring the static CA, dynamic CA and sliding angle. The S1 surface is not superhydrophobic; the water contact angle on this surface is 125° and water droplets adhere firmly not exhibiting slip. The raised areas (i.e.posts) result from pores in the mesh and so occupy 41% of the surface area (Table 1) whereas the height of the posts ranges from 25 to 45 μm, comparable to the diameter of the template wires. The contact angle of a water droplet on this surface is 20° larger than the CA on a flat LDPE surface (105°). This increased

CA, relative to smooth LDPE, is consistent with the additional roughness introduced by embossing as calculated using the Wenzel equation ($\cos\theta_{W^*} = r\cos\theta$),[4] where r, the roughness parameter (ratio of the actual area to the projected area) was estimated to be ~2.2, and θ, the contact angle of a flat LDPE surface, was measured to be 105°. The calculated Wenzel CA is 125°, in good agreement with our measurements.

Surfaces S2−S6 show good superhydrophobicity immediately after processing without any chemical surface modification. The wetting properties of 10 μL water droplets are similar on all four of these surfaces, even though the size and pitch of the surface features is quite different. As shown in Table 2, the static water CAs were measured to be 160°, 159°, 160°, 158° and 160°, respectively. The advancing and receding CA were also measured, and the contact angle hysteresis (CAH = $\theta_{Adv} - \theta_{Rec}$) of surfaces S4 and S6 were calculated to be 8° and 5°, respectively. Water droplets with a volume ≥ 10 μL were difficult to place and could easily roll off these surfaces. The slip angles of a 10 μL droplet on surfaces S2−S6 were 3, 5, 5, 3, and 5°, respectively. These low slip angle values are consistent with previous studies,[10−16] and demonstrate the correlation between a low slip angle and low CAH.

The observed low sliding angles of the fabricated surfaces S2−S6 indicate the drag force generated from the liquid−solid interface is small. It is reasonable to deduce that the droplets rest on top of the spiked surface features and that the ratio of the liquid−air to liquid−solid contact area is large and consistent with the Cassie−Baxter relationship. Submersion of the surface into water entraps a layer of air between the LDPE surface and water which is readily observable. This air layer further corroborates the stability of the Cassie−Baxter state. Though the fabricated polymer posts show an obvious unidirectional slope angle, the surface does not exhibit any measurable anisotropic slip properties. Other studies[39,40] have shown that partial wetting of the posts (i.e., partial Wenzel character) is required to achieve anisotropic slip angles. In this study, it may be that a combination of the high CA (~105°) of PE and high post density could keep the water droplet primarily on the topmost surface of the polymer posts and thus water droplet motion is not influenced by the underlying post slope. As a result, the drag force from the liquid−solid interface is very small, and water droplets can easily roll off the surface in any direction.

3.3. Abrasion-Resistant Properties. The robustness of the fabricated surfaces was evaluated through a series of abrasion tests. First, the surfaces were assessed qualitatively by simply pressing with a bare hand. It was found that the superhydrophobicity of surfaces S2 and S5 decreased dramatically as water droplets were pinned in the touched area, while the superhydrophobicity of surfaces S3, S4, and S6 remained unchanged after pressing with a bare hand as shown in Figure 5a (surface S6). The relative lack of stability of surfaces S2 and S5 is consistent with their structure. Surface S2 has relatively thin petal-like features, whereas S5 has a very low concentration of small features. Both can be easily damaged. In contrast, surfaces S3, S4, and S6 have a higher surface density of larger features. The chemical and abrasion resistance of surfaces S4 and S6 was then studied further using a manual, multistep test that includes a sequence of four steps (including dry abrading with a nitrile and cotton gloved hand and abrading in an industrial cleaning solution with a gloved hand as well as by ultrasonication). After this sequence of tests, the surfaces were rinsed with tap water and dried with filtered dry compressed air. To our surprise, the superhydrophobicity of the two surfaces remained unchanged. As can be seen in Figure 5b,

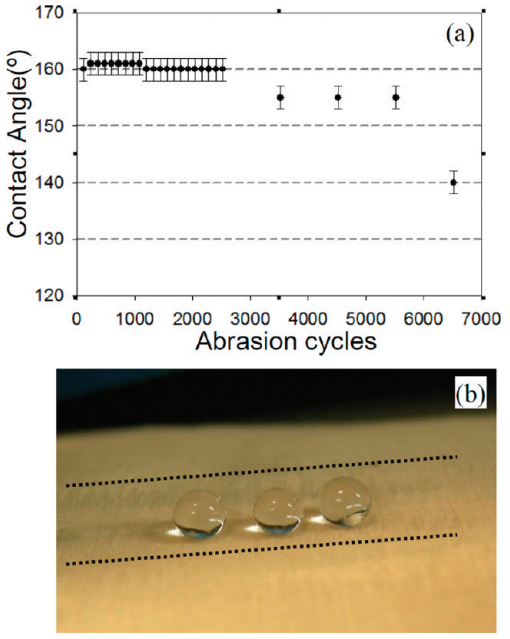

Figure 6. (a) Water contact angle of superhydrophobic surface as a function of abrasion cycles using the Taber reciprocating abraser with a pressure of 32.0 kPa, (b) water droplets on a surface after 2000 cycles of mechanical abrasion testing. The abrasion region lies between the two parallel dashed lines.

two water droplets maintain a spherical shape on surface S6, which had been only partially dried with compressed air after testing. The static water CAs of surfaces S4 and S6 remained essentially unchanged as shown in Figure 5c. The slip angles of 10 μL water droplets on the tested surfaces increased slightly from 5° to 10°. The increased slip angle may result from a partial disordering of the polymer posts after these abrading and scrubbing tests as shown in Figure 5d. The disorder would result in posts of varying heights and so at least some posts may be partially wetted by water droplets, increasing the drag force.

To fully study the robustness of the lamination-templated surfaces, we used a standard reciprocating testing machine to measure the abrasion resistance of surface S4. Testing was performed with a loaded pressure of 32.0 kPa and a linear abrasion speed of 8 cm s^{-1}. The change in static CA on surface S4 with increasing abrasion cycles is shown in Figure 6a. As seen in this figure, the static CA remains essentially unchanged at 160° over the first 2520 abrasion cycles and then decreases slowly to 155° with increasing cycles. The slip angle remains unchanged after 2520 cycles and increases slowly with increasing abrasion cycles. After 5520 cycles, water droplets on the surface still appear as transparent balls (Figure 6b). When the total number of abrasion cycles is increased to 6520, the CA decreased to 140° and then maintained this level with further abrasion cycles. Both the manual multistep test and the mechanized reciprocating test demonstrate that the superhydrophobic surfaces possess good mechanical and chemical stability as well as excellent abrasion resistance.

The high abrasion resistance of these surfaces may be due to the toughness and density of the polymer features which are monolithic with the LDPE film. The micropost surface features were formed during peeling the mesh template from the polymer

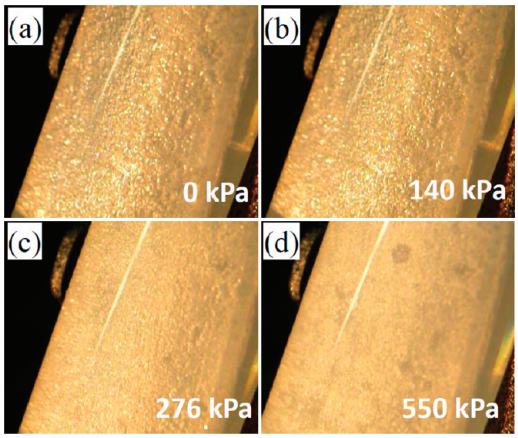

Figure 7. Optical micrographs of surface S2 after immersion in water for at least 90 s within a polypropylene syringe barrel at an applied pressure of (a) 0, (b) 140, (c) 276, and (d) 550 kPa. The air layer formed at the polymer−water interface is reflective creating a mirror effect which persisted to pressures exceeding 550 kPa.

at room temperature. It is well-known that stretching polyethylene at room temperature (elongation-to-break is ∼300%) increases the % crystallinity of the polymer, which in turn, increases the material toughness.[41,42] Since all surfaces were made from LDPE, the significant difference in the robustness between surfaces S2 and S5 vs surfaces S3, S4, and S6 indicates that the dimensions and pitch of the micropost structures also have a strong influence on the robustness of the fabricated superhydrophobic surfaces.

3.4. Water Pressure Stability. In addition to chemical stability and abrasion resistance, the ability to maintain superhydrophobic properties under high static water pressures is another attribute required for commercial applications.[43] To assess the hydrostatic stability of the templated surfaces, the reflectivity of the air layer trapped between surface and the water was observed as a function of applied pressure. A superhydrophobic surface traps a thin layer of air[44,45] at the interface with water. Due to the change in refractive index, this interface is reflective (mirrorlike) and can easily be observed visually and documented with a digital camera. When no pressure is applied, the liquid is in the Cassie state and the triple contact line (TCL) is located near the tips of the surface features, as shown schematically in Figure SF5a. The low slip angle measured for water droplets on this surface (Table 2) is consistent with a small TCL. As the hydrostatic pressure is increased, a partial transition from Cassie to Wenzel would occur and the TCL would descend into the features,[46] decreasing the reflectivity as shown in SF5b&c.

The stability of surface S2 was evaluated by placing it within a syringe barrel, immersing it into water and pressuring the syringe with compressed air. It can be seen from Figure 7 that the reflectivity remains relatively stable to 140 kPa of applied pressure, but the reflected intensity gradually becomes weaker with increasing pressure. The reflective interface significantly fades when the applied pressure was increased to 550 kPa over a period of 90 s, indicating a partial transition from Cassie to Wenzel states. Small, dark regions seen in Figure 7d may be isolated areas of complete transition to the Wenzel state. The reduction of the reflectivity at 550 kPa is not, however, permanent. The reflectivity can be restored by removing the sample and drying with compressed air. The loss of reflectivity at higher pressures is due to a transition to a partial Wenzel state (i.e., the TCL descends from the tips toward the base of the surface), and not due to solubility of air into the water, because we have observed stable air layers at 550 kPa for long times (>24 h) using the same technique on other types of superhydrophobic surfaces we fabricated. These surfaces are composed of submicrometer surface features and so would be expected to exhibit greater stability under pressure.

At lower pressures, the air layer remained intact for extended periods of time. At 55 kPa (equal to 8 psi or the pressure at a depth of 5.6 m of water), the surface remained completely dry when it was removed after 5 h of under-water immersion. This indicates that the templated LDPE surface is able to effectively trap air and maintain superhydrophobic properties underwater for extended periods of time.

The water pressure stability of these surfaces is significantly greater than natural superhydrophobic surfaces. For example, the transition from the Cassie−Baxter to the Wenzel state on a lotus leaf occurs at 13.5 kPa (<2 psi).[45] The performance of the lamination-templating materials reported here is also significantly better than other reported polymeric superhydrophobic surfaces;[47] however, some laser-scribed aluminum surfaces have been reported to be stable at pressures above 690 kPa.[44]

4. CONCLUSION

Superhydrophobic polymer surfaces with excellent abrasion resistance and water pressure stability were successfully fabricated using a simple and inexpensive lamination templating method. The structure of the 3D ordered microposts can be easily controlled by adjusting the lamination conditions (pressure, temperature, and time) and/or by changing the type of mesh template used. Using a lamination temperature above the crystalline melt temperature of the thermoplastic polymer insures that the polymer can fully infiltrate into the open, porous template. Peeling the surface after lamination elongates the polymer material that had infiltrated the pores, creating a 3D array of high-aspect-ratio posts. The fabricated polymer surfaces exhibit superhydrophobicity immediately after peeling, without any subsequent chemical surface modification.

These templated LDPE surfaces exhibit stable superhydrophobic properties after numerous tests. The surfaces exhibit good underwater stability as they remain dry after immersion in water for 5 h at a pressure of 55 kPa. They are robust to both chemical cleaning and mechanical abrasion with a gloved hand. Moreover, the surfaces retain superhydrophobic properties after more than 5500 cycles in a standard mechanical reciprocating abrasion machine under an applied pressure of 32.0 kPa. This abrasion resistance is significantly greater than any previously reported superhydrophobic surface. Future work will focus on defining the relationship between polymer properties, surface morphology and the mechanical robustness of the surface.

The lamination templating method is environmental friendly as it is completely free of organic solvents or noxious chemicals and recycled LDPE can be used. Although we only report results for LDPE, we have used other polymers to fabricate superhydrophobic surfaces with this approach. A significant advantage of the present method is that the meshes used as templates are commercially available in large rolls and in a variety of sizes and patterns. In addition, the woven mesh templates are reusable, unlike methods that employ sacrificial templates such as anodized aluminum or other materials. Thus the lamination templating

method may provide an economically viable path to manufacture large areas of mechanically robust superhydrophobic surfaces from inexpensive polymers.

■ ASSOCIATED CONTENT

Supporting Information. A DSC curve of the LDPE thermal transitions is shown in SF1, photographs of the Taber linear abraser test are shown in SF2, a schematic illustration of the static pressure test is shown in SF3, an SEM perspective view of surface S1 is shown in SF4 and a schematic illustration of the effect of static pressure on the position of the TCL and the reflectivity at the air—water interface is shown in SF5. This material is available free of charge via the Internet at http://pubs.acs.org.

■ AUTHOR INFORMATION

Corresponding Author
*E-mail: alan.lyons@csi.cuny.edu.

■ ACKNOWLEDGMENT

This research was supported by the New York State Foundation for Science, Technology and Innovation (NYSTAR) Faculty Development Program. Additional support was received from the NYSTAR funded Center for Engineered Polymeric Materials. We thank Zhantong Mao and Mark Barahman for helpful discussions.

■ REFERENCES

(1) Barthlott, W.; Neinhuis, C. *Planta* **1997**, *202*, 1–8.
(2) Gao, X.; Jiang, L. *Nature* **2004**, *432*, 36.
(3) Quere, D. *Annu. Rev. Mater. Res.* **2008**, *38*, 71–99.
(4) Wenzel, R. N. *Ind. Eng. Chem.* **1936**, *28*, 988–994.
(5) Cassie, A. B. D.; Baxter, S. *Trans. Faraday Soc.* **1944**, *40*, 546–551.
(6) Gao, L. C.; McCarthy, T. J. *Langmuir* **2009**, *25*, 14105–14115.
(7) Extrand, C. W. *Langmuir* **2002**, *18*, 7991–7999.
(8) Gao, L. C.; McCarthy, T. J. *Langmuir* **2006**, *22*, 2966–1967.
(9) Chen, M. H.; Hsu, T. H.; Chuang, Y. J.; Tseng, F. G. *Appl. Phys. Lett.* **2009**, *95*, 023702.
(10) Koch, K.; Bhushan, B.; Barthlott, W. *Soft Matter* **2008**, *4*, 1943–1963.
(11) Li, X. M.; Reinhoudt, D.; Crego-Calama, M. *Chem. Soc. Rev.* **2007**, *36*, 1350–1368.
(12) Yao, X.; Song, Y.; Jiang, L. *Adv. Mater.* **2011**, *23*, 719–734.
(13) Xue, C. H.; Jia, S. T.; Zhang, J.; Ma, J. Z. *Sci. Technol. Adv. Mater.* **2010**, *11*, 033002.
(14) Bhushan, B.; Jung, Y. C. *Prog. Mater. Sci.* **2010**, *56*, 1–108.
(15) Crick, C. R.; Parkin, I. P. *Chem.—Eur. J.* **2010**, *16*, 3568–3588.
(16) Lafuma, A.; Quere, D. *Nat. Mater.* **2003**, *2*, 457–460.
(17) Xu, Q. F.; Wang, J. N.; Smith, I. H.; Sanderson, K. D. *J. Mater. Chem.* **2009**, *19*, 655–660.
(18) Lee, Y.; Ju, K. Y.; Lee, J. K. *Langmuir* **2010**, *26*, 14103–14110.
(19) Xu, Q. F.; Wang, J. N.; Sanderson, K. D. *Acs. Nano* **2010**, *4*, 2201–2209.
(20) Bravo, J.; Zhai, L.; Wu, Z.; Cohen, R. E.; Rubner, M. F. *Langmuir* **2007**, *23*, 7293–7298.
(21) Zhang, X.; Shi, F.; Niu, J.; Jiang, Y.; Wang, Z. *J. Mater. Chem.* **2008**, *18*, 621–633.
(22) Sethi, S.; Dhinojwala, A. *Langmuir* **2009**, *25*, 4311–4313.
(23) Levkin, P. A.; Svec, F.; Fréchet, J. M. J. *Adv. Funct. Mater.* **2009**, *19*, 1–6.
(24) Xu, Q. F.; Wang, J. N. *New J. Chem.* **2009**, *33*, 734-738.
(25) Zhai, L.; Cebeci, F. C.; Cohen, R. E.; Rubner, M. F. *Nano Lett.* **2004**, *4*, 1349–1353.
(26) Tuteja, A.; Choi, W.; Mabry, J. M.; McKinley, G. H.; Cohen, R. E. *Proc. Natl. Acad. Sci. U.S.A.* **2008**, *105*, 18200–18205.
(27) Tuteja, A.; Choi, W.; Ma, M. L.; Mabry, J. M.; Mazzella, S. A.; Rutledge, G. C.; McKinley, G. H.; Cohen, R. E. *Science* **2007**, *318*, 1618–1622.
(28) Tuteja, A.; Choi, W. J.; McKinley, G. H.; Cohen, R. E.; Rubner, M. F. *MRS Bull.* **2008**, *33*, 752.
(29) Chhatre, S. S.; Choi, W.; Tuteja, A.; Park, K. C.; Mabry, J. M.; Mckinley, G. H; Cohen, R. E. *Langmuir* **2010**, *26*, 4027–4035.
(30) Darmanin, T.; Guittard, F. *J. Mater. Chem.* **2009**, *19*, 7130–7136.
(31) Deng, B.; Cai, R.; Yu, Y.; Jiang, H.; Wang, C.; Li, J.; Li, L.; Yu, M.; Li, J.; Xie, L.; Huang, Q.; Fan, C. *Adv. Mater.* **2010**, *22*, 5473–5477.
(32) Xu, Q. F.; Wang, J. N.; Sanderson, K. D. *J. Mater. Chem.* **2010**, *20*, 5961–5966.
(33) Artus, G. R. J.; Jung, S.; Zimmermann, J.; Gautschi, H.; Marquardt, K.; Seeger, S. *Adv. Mater.* **2006**, *18*, 2758–2762.
(34) Park, S. H.; Lee, S. M.; Lim, H. S.; Han, J. T.; Lee, D. R.; Shin, H. S.; Jeong, Y.; Kim, J.; Cho, J. H. *ACS Appl. Mater. Interfaces* **2010**, *2*, 658–662.
(35) Budunoglu, H.; Yildirim, A.; Guler, M. O.; Bayindir, M. *ACS Appl. Mater. Interfaces* **2011**, *3*, 539–545.
(36) Su, C. H.; Xu, Y. Q.; Gong, F.; Wang, F. S.; Li, C. F. *Soft Mater* **2010**, *6*, 6068–6071.
(37) Xiu, Y. H.; Liu, Y.; Hess, D. W.; Wong, C. P. *Nanotechnology* **2010**, *21*, 155705.
(38) Jin, M. H.; Feng, X. J.; Feng, L.; Sun, T. L.; Zhai, J.; Li, T. J.; Jiang, L. *Adv. Mater.* **2005**, *17*, 1977–1981.
(39) Barahman M.; Lyons, A. M. *Langmuir* [Online early access], DOI 10.1021/la201222a. Published on line: June 23, 2011.
(40) Kusumaatmaja, H.; Yeomans, J. M. *Soft Matter* **2009**, No. 5, 2704–2707.
(41) Galeski, A. *Prog. Polym. Sci.* **2003**, *28*, 1643–1699.
(42) Seguela, R. *J. Macromol. Sci. C* **2005**, *45*, 263–287.
(43) Boinovich, L.; Emelyanenko, A. M.; Pashinin, A. S. *ACS Appl. Mater. Interfaces* **2010**, *2*, 1754–1758.
(44) Peguero C. On the Manufacture and Application of Superhydrophobic Surfaces for Skin Friction Reduction in Laminar and Turbulent Flows. *Ph. D. Thesis*, Brown University, Providence, RI, May 2011
(45) Sheng, X. L; Zhang, J. H. *Colloids Surf., A* **2011**, *377*, 374–378.
(46) Lobaton, E. J.; Salamon, T. R. *J. Colloid Interface Sci.* **2007**, *314*, 184–198.
(47) Poetes, R.; Holtzmann, K.; Franze, K.; Steiner, U. *Phys. Rev. Lett.* **2010**, *105*, 166104.